

ORIGINAL ARTICLE

Kinome siRNA-phosphoproteomic screen identifies networks regulating AKT signaling

Y Lu^{1,5}, M Muller^{1,5}, D Smith¹, B Dutta¹, K Komurov¹, S Iadevaia¹, D Ruths², J-T Tseng¹, S Yu¹, Q Yu¹, L Nakhleh², G Balazsi¹, J Donnelly³, M Schurdak³, S Morgan-Lappe³, S Fesik^{3,4}, PT Ram^{1,5} and GB Mills^{1,5}

¹Department of Systems Biology, UT MD Anderson Cancer Center, Houston, TX, USA; ²Computer Science Department, Rice University, Houston, TX, USA and ³Global Pharmaceutical Research and Development, Abbott Laboratories, Abbott Park, IL, USA

To identify regulators of intracellular signaling, we targeted 541 kinases and kinase-related molecules with small interfering RNAs (siRNAs), and determined their effects on signaling with a functional proteomics reverse-phase protein array (RPPA) platform assessing 42 phospho and total proteins. The kinome-wide screen demonstrated a strong inverse correlation between phosphorylation of AKT and mitogen-activated protein kinase (MAPK) with 115 genes that, when targeted by siRNAs, demonstrated opposite effects on MAPK and AKT phosphorylation. Network-based analysis identified the MAPK subnetwork of genes along with p70S6K and FRAP1 as the most prominent targets that increased phosphorylation of AKT, a key regulator of cell survival. The regulatory loops induced by the MAPK pathway are dependent on tuberous sclerosis complex 2 but demonstrate a lesser dependence on p70S6K than the previously identified FRAP1 feedback loop. The siRNA screen also revealed novel bi-directionality in the AKT and GSK3 (Glycogen synthase kinase 3) interaction, whereby genetic ablation of GSK3 significantly blocks AKT phosphorylation, an unexpected observation as GSK3 has only been predicted to be downstream of AKT. This method uncovered novel modulators of AKT phosphorylation and facilitated the mapping of regulatory loops.

Oncogene (2011) 30, 4567–4577; doi:10.1038/onc.2011.164; published online 13 June 2011

Keywords: AKT; MAPK; proteomics; signaling networks; siRNA

Introduction

Cancer-causing mutations frequently alter homeostatic signaling, leading to increased cell proliferation and

survival (Hanahan and Weinberg, 2000; Hunter, 2000). Activating mutations target multiple components of the phosphatidylinositol 3-kinase (PI3K)/AKT (aka PKB) pathway in a greater number of tumors than any other signaling pathway, emphasizing the importance of the PI3K/AKT pathway in tumor initiation and progression (Brugge *et al.*, 2007). Based on the importance of the PI3K/AKT pathway, many small-molecule inhibitors targeting this pathway are in preclinical and early clinical evaluation (Hennessy *et al.*, 2005).

The upstream regulators and downstream targets of AKT are diverse (Engelman *et al.*, 2006; Manning and Cantley, 2007). Phosphorylation and activation of AKT can be achieved through activation of receptor tyrosine kinases, as well as G protein-coupled receptors (Engelman *et al.*, 2006). Regulatory loops have been proposed to maintain pathway homeostasis. One well-characterized negative feedback loop involves the tuberous sclerosis complex (TSC), the Rheb RAS superfamily member, the kinase mTOR, the mTOR target p70 ribosomal S6 kinase (p70S6K) that inhibits insulin receptor substrate 1 and insulin-like growth factor receptor signaling (Manning *et al.*, 2005; Avruch *et al.*, 2006; O'Reilly *et al.*, 2006).

An improved understanding of the homeostatic mechanisms that control the PI3K/AKT pathway is required to efficiently implement targeted therapeutics and, in particular, to facilitate the design of rational therapeutic combinations that bypass the effects of homeostatic loops. To address this gap in knowledge, we used a systems approach that combined a screen of 540 siRNA pools targeting kinases and related molecules with a high-throughput functional proteomics RPPA platform (Tibes *et al.*, 2006; Amit *et al.*, 2007; Muller *et al.*, 2008; Iadevaia *et al.*, 2010) assessing the abundance of 42 phosphorylated and parental proteins. This analysis revealed an inverse correlation between AKT and mitogen-activated protein kinase_{1,2} (MAPK_{1,2}) phosphorylation, as well as new feedback loops within the AKT–MAPK network.

Results

To identify regulators of the PI3K/AKT pathway, we used a systems approach combining a screen of 541

Correspondence: Dr PT Ram, Department of Systems Biology, UT MD Anderson Cancer Center, 7435 Fannin St, Houston, TX 77054, USA. E-mail: pram@mdanderson.org

⁴Current address: Vanderbilt-Ingram Cancer Center, Vanderbilt University, Nashville, TN, USA.

⁵These authors contributed equally to this work.

Received 5 November 2010; revised and accepted 5 April 2011; published online 13 June 2011

Table 1 Details of siRNA kinome screen

No. of siRNA targets in primary screen	541
No. of pooled siRNAs targeting each gene	4
No. of conditions per siRNA	2
No. of repeats per siRNA	3
No. of antibodies in RPPA	42
No. of dilutions per sample on RPPA	5
Total no. of assayed points in siRNA-RPPA screen	~682 500
No. of gene targets re-tested	18
No. of cell lines re-tested	5
No. of different conditions per cell line tested	12
No. of phospho and total proteins assayed in each cell line	6–10
Total no. of data points assayed to validate primary screen	~2600

Abbreviations: RPPA, reverse-phase protein array; siRNA, small interference RNA.

Table 2 Details of validation of siRNA screen

No. of siRNAs in screen	541
No. of siRNA targets assayed for protein expression by RPPA in screen	15
No. (percent) of successful knockdowns in screen (measured by RPPA)	10/15 (67%)
No. of genes targeted that decreased pAKT in screen (z -score < -1.4)	34
No. of genes targeted that increased pAKT in screen (z -score > 1.4)	15
No. of gene targets re-validated using different siRNA sequences	18
No. (percent) of genes that re-confirmed knockdown with different siRNAs	13/18 (72%)
No. (percent) of genes targeted that re-confirmed change in pAKT with different siRNAs	10/13 (77%)
No. (percent) of genes targeted that showed no change in pAKT with different siRNAs	2/13 (15%)
No. (percent) of genes targeted that showed opposite change in pAKT with different siRNAs	1/13 (8%)

Abbreviations: RPPA, reverse-phase protein array; siRNA, small interference RNA.

siRNA pools targeting kinases and related molecules (Table 1 and Supplementary Table 1) with the RPPA platform against phospho and total forms of 25 different proteins (Supplementary Table 2). The screen was performed in the MDA-MB-468 cell line, which, owing to overexpression of the epidermal growth factor receptor (EGFR) and mutational inactivation of PTEN, has high constitutive activation in the PI3K/AKT pathway.

Protein abundance for 15 of the siRNA targets was available on the RPPA array to validate knockdown (Table 2). Of the 15 targets assessed, all but 3 were significantly decreased by at least one isogenic siRNA (Supplementary Table 3) when the cells were exposed to specific siRNAs, but not by nontargeting siRNA or other siRNA pools assessed. We observed a 60–70% knockdown efficiency based on the siRNA–RPPA pairs (10/15) as well as revalidation studies (13/18); these numbers are in line with previous siRNA screens as reported by other investigators (MacKeigan *et al.*, 2005; Berns *et al.*, 2007). In the case of AKT and GSK3 (Glycogen synthase kinase 3), for which multiple isoforms exist, at least one of the siRNAs knocked down the target. As the antibodies assessed recognize all

AKT and GSK3 isoforms, this likely represents targeting of the dominant isoforms in the MDA-MB-468 breast cancer cell line model used in the screen. For example, MDA-MB-468 cell line expressed higher levels of AKT1 and AKT3 than AKT2 and knockdown of only these two isoforms decreased total AKT protein levels (Supplementary Table 3 and Supplementary Figure 1).

Because of the importance of the PI3K/AKT pathway in breast cancer (Neve *et al.*, 2006; Brugge *et al.*, 2007), we determined which siRNAs altered AKT phosphorylation (phospho-AKT (pAKT)) at S⁴⁷³ and T³⁰⁸ in serum-starved MDA-MB-468 cells (EGFR overexpressed, PTEN mutant) using a z -score of ± 1.4 for the average change in both AKT phosphosites for significance (Figure 1a and Table 1). In all, 34 of the 541 targeted kinase and kinase-associated proteins decreased the abundance of pAKT (including AKT1 and AKT3 siRNAs, green in Supplementary Table 4), whereas 15 increased the abundance of pAKT (red in Supplementary Table 4). We identified five known upstream modifiers of AKT phosphorylation, including receptors, intracellular kinases and PI3K isoforms, eight downstream effectors, as well as 34 genes not previously related to AKT function (Supplementary Table 4; AKT1 and AKT3 are not counted as up- or downstream, bringing the total to 49). The sequences of these siRNA are shown in Supplementary Table 5.

The 15 siRNAs that increased pAKT could target negative regulators acting upstream of AKT or potentially components of feedback loops. With PathwayOracle (Ruths *et al.*, 2008a, b), we reconstructed a directed signaling network based on published literature (PubMed) to identify possible pathways accounting for the increase in pAKT levels. Of the 15 siRNAs that increased the abundance of pAKT, 3 of the siRNA targets were predicted to increase pAKT phosphorylation based on existing literature (Supplementary Table 4). These included siRNAs targeting *MAP2K4*, which encodes a mitogen-activated protein kinase kinase kinase upstream of JNK (Song and Lee, 2005), *RPS6KB1*, which encodes p70 ribosomal S6 kinase (p70-S6K) (O'Reilly *et al.*, 2006), and Raf1, which is upstream of MAPK (Buck *et al.*, 2008); this is consistent with the known actions of these proteins with respect to AKT.

To capture the information contained in the data, we implemented a network-based approach probing three protein–protein interaction databases (HPRD (Human Protein Reference Database) (<http://www.hprd.org>), BIND (Biomolecular Interaction Database) (<http://www.bind.ca>) and TRANSPATH (<http://www.biobase-international.com>)) for the connectivity of the siRNA targets and AKT. Using a z -score of ± 1.4 (assigned based on the change in shape of the curve) for effects on the average abundance of pAKT S473 (Figure 1b) and pAKT T308 (Figure 1c) phosphosites, the only interconnected genes that when targeted increased the abundance of pAKT were found to be components of the MAPK network. To explore the entire data set and not assign any cut-off values, we used

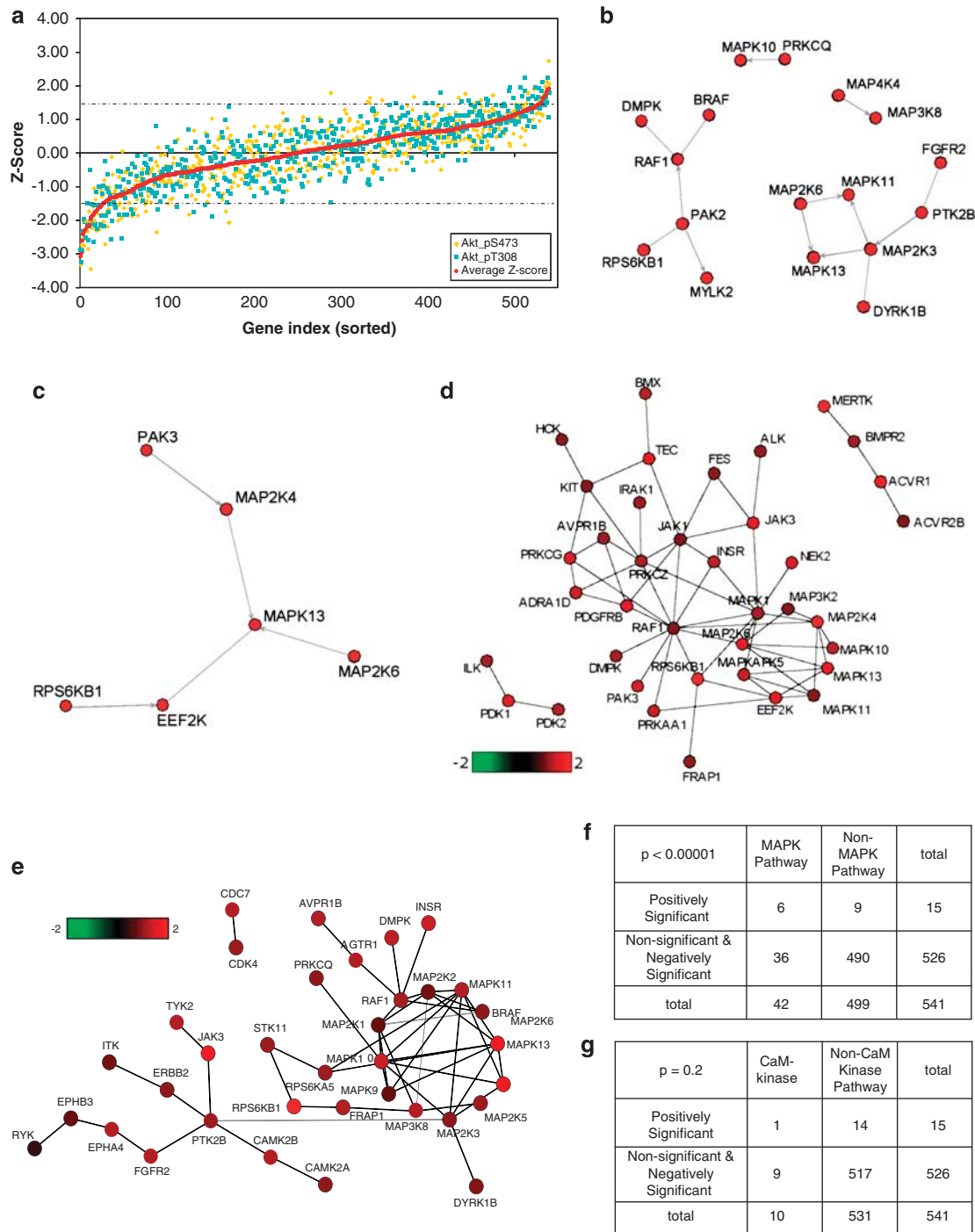


Figure 1 (a) Scatter plot of changes in phospho Ser473 (yellow), Thr308 (blue) and average of the two phosphor sites (red) of AKT in response to siRNA. The siRNAs are plotted individually on the x-axis and the z-score of Akt phosphorylation is plotted on the y-axis. (b) Network of genes that when targeted by siRNA increased phospho-Ser473 AKT above 1.7 z-score. (c) Network of genes that when targeted by siRNA increased phospho-Thr308 AKT above 1.7 z-score. (d) The most high scoring networks from the NetWalk analysis of the genes that when targeted by siRNA increased Ser473 AKT phosphorylation. (e) The most high scoring networks from the NetWalk analysis of the genes that when targeted by siRNA increased Thr308 AKT phosphorylation. (f) Enrichment of MAPK genes in the total set of siRNA targets. Statistical analysis of all MAPK family genes targeted in the siRNA screen and their effect on the abundance of phosphorylated AKT shows a significant role of MAPK pathway in regulating AKT. (g) Targeting casein kinase A1 (CSNK1A1 in 2A) produced the fourth highest increase in AKT phosphorylation; however, statistical analysis of the casein kinase pathway in the screen showed no significant increase in AKT phosphorylation.

a random walk network-based approach using NetWalk (Komurov *et al.*, 2010b). Analysis of the entire data set revealed that the MAPK module was the largest

subnetwork of genes that increased AKT phosphorylation at T308 and S473 (Figures 1d and e). NetWalk analysis also identified three members of the CaMK

network as genes that when targeted increased AKT phosphorylation at S473 (Figure 1e). The two phospho-sites act coordinately on AKT activity. Therefore, we averaged the data from the two phospho-sites of AKT and statistically re-analyzed the data. Strikingly, 6 out of the 15 genes that, when targeted, increased pAKT on both phosphorylation sites were members of the MAPK signaling network (Supplementary Table 1). Statistical analysis of averaging the two phosphosites revealed a significant enrichment of MAPK pathway genes ($P < 0.0001$, χ^2 test, Figure 1f) as compared with all other genes in the siRNA screen. To determine if the effect of targeting the MAPK pathway on increasing pAKT was specific, we assessed calcium-calmodulin kinase pathways ($P = 0.2$, χ^2 test, Figure 1g) but failed to identify a significant enrichment, supporting the argument that the MAPK and AKT pathways are highly interrelated.

Analysis of the abundance of phosphorylated MAPK1,2 and phosphorylated AKT across all siRNA targets showed a clear negative correlation between AKT and MAPK1,2 phosphorylation (Figure 2a and Supplementary Table 6). Regression analysis of the tails of the AKT and MAPK response curves and their intersections revealed 115 siRNAs that showed a significant inverse correlation coefficient of ≥ -0.50 , suggesting that the MAPK and AKT pathways are tightly counterbalanced with potentially extensive negative crosstalk. Multiple siRNAs targeting members of the MAPK pathways (MAPK1,2, p38 and JNK) increased AKT phosphorylation (Supplementary Table 1). To validate the siRNA screen, we independently decreased MAPK2 and MEK1 abundance using different siRNA sequences and repeated the experiment in a different breast tumor cell line MDA-MB-231, which contains a mutation in genes encoding Ras and Raf, thus resulting

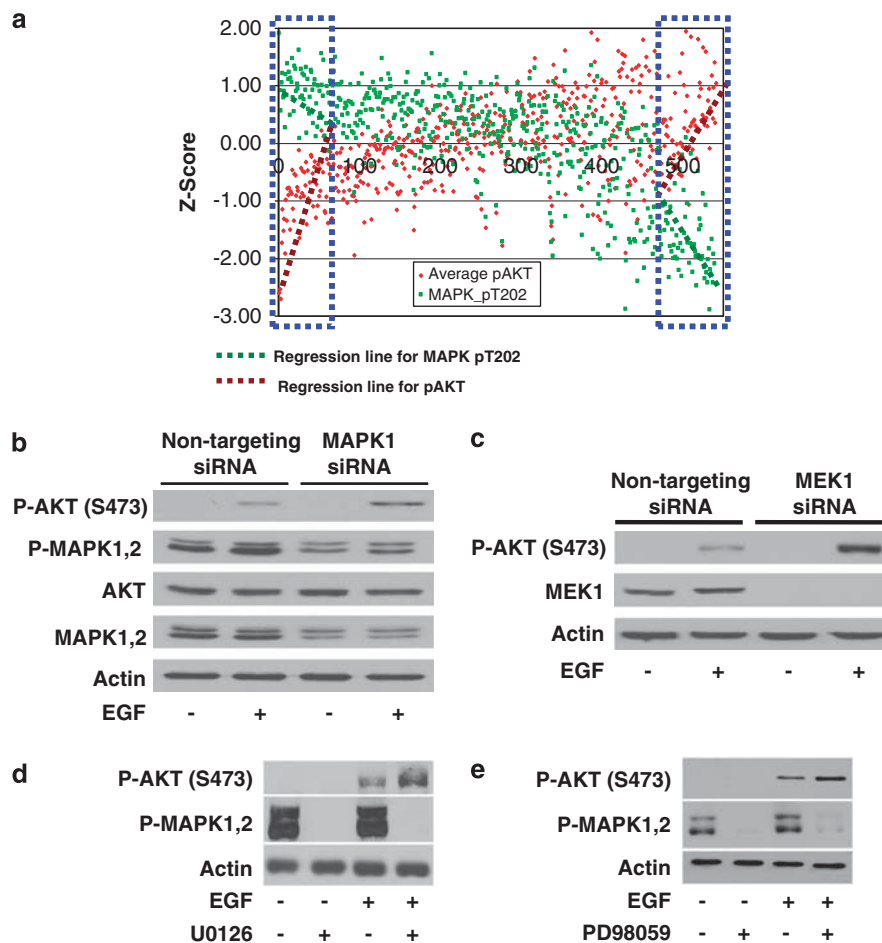


Figure 2 (a) AKT and MAPK phosphorylation are inversely correlated. Regression analysis of AKT and MAPK phosphorylation in response to the same siRNA reveals that 115 siRNAs have significant inverse correlation ($r = -0.5$) in their effect on the phosphorylation of AKT and MAPK (see Supplementary Table S5 for the list of siRNA targets and their alteration of MAPK1,2 phosphorylation). (b) siRNA targeting of MAPK1 in an independent cell line (MDA-MB-231) shows increase in phosphorylation of Thr473 of AKT when MAPK1 is knocked down. (c) siRNA targeting of MEK1, which is upstream of MAPK, in MDA-MB-231 cells also increases AKT phosphorylation when MEK1 is knocked out. (d, e) Inhibition of MEK with different MEK inhibitors increases AKT phosphorylation. MDA-MB-231 cells were serum starved and incubated with MEK inhibitor U0126 (d) or PD98059 (10 μ M) (e) for 1 h before stimulation with EGF (20 ng/ml) for 10 min. Cell lysates were probed for phosphorylated AKT. (f, g) MDA-MB-468 (f) and MDA-MB-231 (g) cells were serum starved and incubated with MEK inhibitor for 1 h before stimulation with EGF (20 ng/ml) for 10 min, cell lysates were probed on the RPPA (heat map of data) and graphs show changes in pAKT in response to conditions as indicated. (h) Immunoprecipitation of individual AKT isoforms shows that AKT1 and AKT3 both show increased phosphorylation in response to EGF and MEK inhibition.

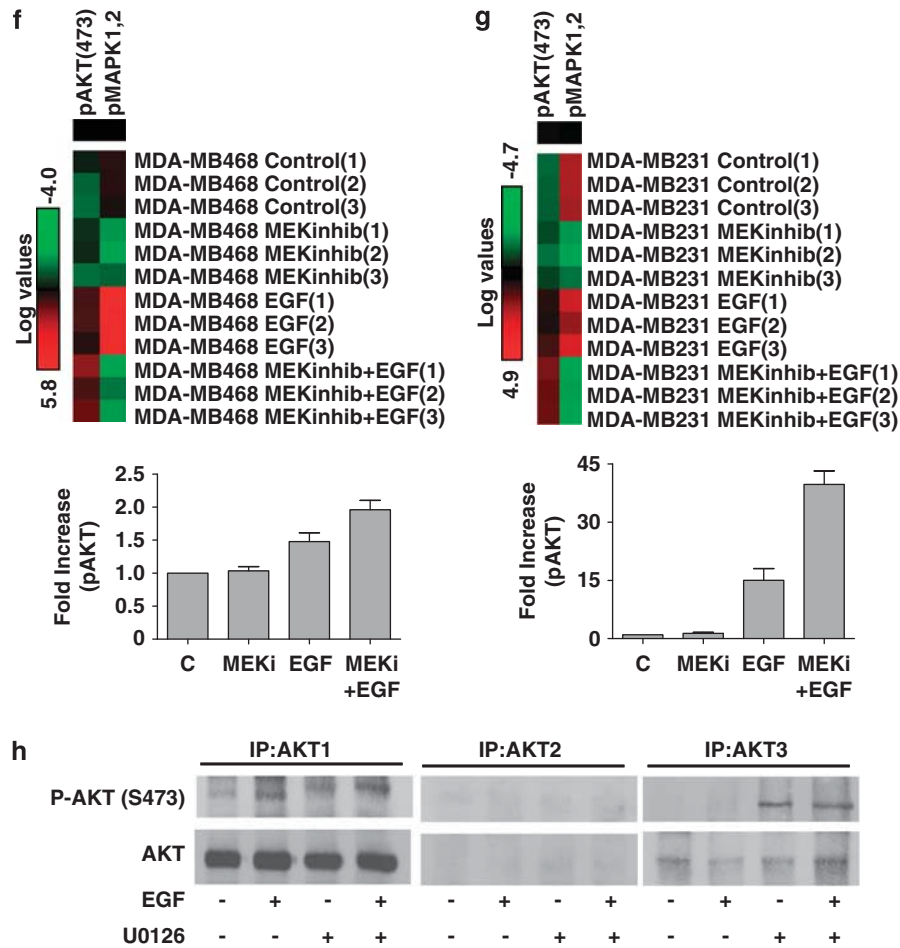


Figure 2 Continued.

in constitutive activation of the MAPK1,2 pathway. As MDA-MB-231 cells have wild-type PTEN, lack EGFR amplification and potentially, owing to the activated MAPK pathway, have no measurable basal AKT phosphorylation, we added epidermal growth factor (EGF) to stimulate AKT phosphorylation and then measured the effects of the siRNAs on AKT phosphorylation. When MAPK1 (p42 MAPK—lower band of p42/p44 doublet on the MAPK blot) or MEK1 was knocked down with an independent siRNA, there was an increase in AKT phosphorylation compared with that in cells transfected with control siRNA (Figures 2b and c). We also validated the effect of siRNAs targeting the MAPK pathway on AKT phosphorylation by applying pharmacological inhibitors of the MAPK pathway. MEK was blocked with two different inhibitors, U2016 and PD98059, in MDA-MB-231 cells, resulting in an increase in AKT phosphorylation in the presence of EGF (Figures 2d and e). We further confirmed that pharmacological inhibitors of MEK could also increase AKT phosphorylation in the MDA-MB-468 cells and our data show that treating cells (MDA 468 and MDA 231) with MEK inhibitor increases AKT phosphorylation (Figures 2f and g). To determine if there was a difference in the phosphorylation of specific AKT isoforms in response to MEK

inhibitors, we determined the expression of the three AKT isoforms. AKT1 and AKT3 (Supplementary Figure 1) are expressed in both cell lines and both isoforms showed increased levels of phosphorylation in the presence of MEK inhibitor (Figure 2h).

To better understand the functional relationship between the target of the siRNA and AKT phosphorylation, we developed a directed network map in PathwayOracle (Ruths *et al.*, 2008a,b) using the published literature of pairwise interactions from PubMed searches and *Science Signaling* (<http://stke.sciencemag.org/cm/>). siRNAs that decreased the abundance of proteins that increased AKT phosphorylation are colored in shades of red, whereas siRNAs that decreased the abundance of proteins that decreased AKT phosphorylation are colored in shades of green. (Figure 3a). The intensity of the color is determined by the corresponding z-scores, and proteins in blue were not assessed with siRNA. siRNA targeting p70S6K and mTOR, which had been previously shown as part of a homeostatic loop (O'Reilly *et al.*, 2006; Wan *et al.*, 2007), increased AKT phosphorylation, thus enhancing confidence in the ability of the siRNA screen to accurately identify feedback loops (Figure 3a and Supplementary Table 1). Previously reported pair-wise interactions show that MAPK1,2 can activate p90RSK,

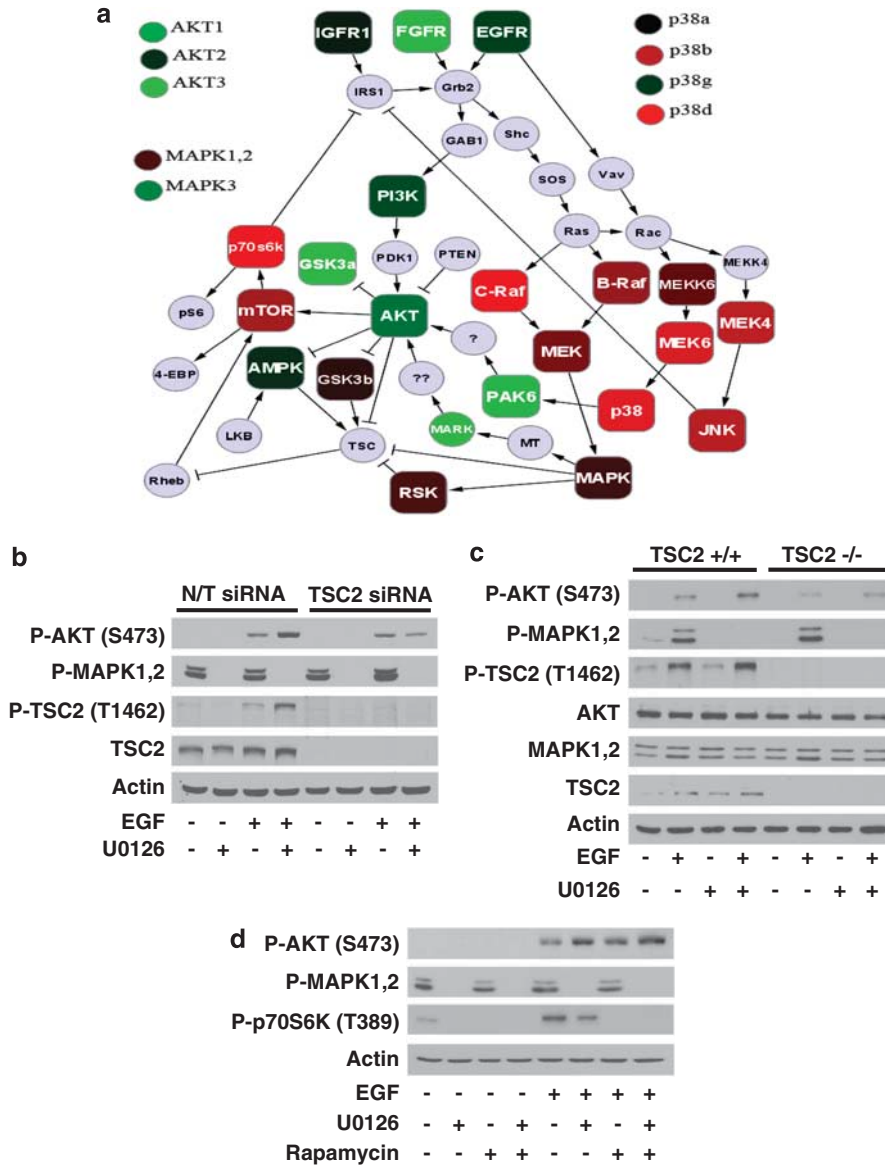


Figure 3 (a) Network model of putative regulatory loops involving AKT. Directed network of the siRNA targets, their interactions and their effect on AKT phosphorylation was developed in PathwayOracle. Nodes in red are those that when targeted increased AKT phosphorylation, nodes in green are those that when targeted produced a decrease in AKT phosphorylation, and nodes in blue were not targeted in the siRNA screen. Shades of red and green indicate z-scores of AKT phosphorylation (see Supplementary Table S3 for corresponding values). (b) TSC2 knockdown in MDA MB-231 cells blocks the increase in AKT phosphorylation induced by inhibition of the MAPK pathway. MDA-MB-231 cells were transfected with SMARTpool TSC2 siRNA for 72 h, followed by MEK inhibitor U0126 for 1 h and stimulated with EGF for 10 min as indicated. Cell lysates were probed for phosphoproteins as indicated. (c) TSC2^{-/-} MEFs have a blunted increase in AKT phosphorylation when the MAPK pathway is inhibited. MEFs from TSC2 wild-type (TSC +/+) and TSC2 knockout (TSC2^{-/-}) animals were serum starved, incubated with MEK inhibitor U0126 for 1 h, and stimulated with EGF for 10 min. Cell lysates were probed for phosphorylated AKT and other kinases as indicated. (d) MDA-MB-231 cells were treated with either MEK inhibitor (U0126) or mTOR inhibitor (rapamycin), or both as indicated. The cells were stimulated with EGF and lysates probed for phospho-AKT, MAPK1,2 and p70S6K. MEK inhibition only partially decreases p70S6K (lane 6) as compared with rapamycin (lane 7), but the increase in pAKT is greater in lane 6 compared to lane 7.

which in turn can phosphorylate TSC2, altering its activity (Roux *et al.*, 2004; Ballif *et al.*, 2005). Additional reports suggest that MAPK1,2 can directly phosphorylate TSC2 (Ma *et al.*, 2005). TSC2 in turn regulates the Rheb-mTOR-S6K feedback loop leading to changes in insulin receptor substrate 1 activity, thus altering AKT phosphorylation (Kwiatkowski and Manning, 2005; Manning *et al.*, 2005; Avruch *et al.*, 2006). We reconstructed

the network in PathwayOracle, modeled the inhibition of MAPK1,2 and measured the changes in AKT phosphorylation, as well as all members of the network. A signaling petri-net model (Ruths *et al.*, 2008a,b) predicted that the negative regulatory Rheb-mTOR-S6K loop from MAPK would increase AKT phosphorylation (Figure 3a) when MEK or MAPK1,2 are inhibited. The model further indicated that knockdown

of TSC2 would decrease the effect of inhibition of MEK on AKT phosphorylation.

We experimentally tested the activation state (based on phosphorylation) of MAPK and AKT in response to depletion of TSC2 by siRNA or gene deletion. As predicted, knockdown of TSC2 with siRNA decreased AKT phosphorylation induced by MEK inhibitors (Figure 3b). In an independent approach to determine whether TSC2 has a role in connecting the MAPK and AKT pathways, we assessed TSC2-knockout mouse embryonic fibroblasts (MEFs). In the TSC2-knockout cells, there was only a 0.6-fold increase in AKT phosphorylation when MEK was inhibited compared with a 2.5-fold increase in TSC2 wild-type cells (Figure 3c). Thus, a TSC2-mediated feedback loop appears to have an important role in connecting MAPK signaling to AKT activity.

Previous studies show a p70S6k-IRS-1-mediated negative feedback loop from mTOR leading to increased AKT phosphorylation (O'Reilly *et al.*, 2006). Recent studies suggest that the MEK/MAPK-mediated regulatory feedback loop to AKT may overlap with the mTOR loop and converge on insulin receptor substrate 1 (Buck *et al.*, 2008). To examine this further, we determined the effect of concurrent MEK inhibition and mTOR inhibition on AKT phosphorylation and found that there was a slightly additive effect, and that the MEK inhibitor-induced increase in AKT phosphorylation is greater than when mTOR is inhibited alone (Figure 3d), suggesting that the MAPK-induced loop may be dominant over the mTOR loop. The data show that rapamycin completely inhibits phospho-p70S6K while inducing the negative feedback loop as previously described (O'Reilly *et al.*, 2006). However, most strikingly, MEK inhibition only partially decreases p70S6K phosphorylation, yet causes a higher increase in AKT phosphorylation, suggesting parallel and overlapping feedback loops to AKT (Figure 3d).

We next analyzed the genes that when targeted by siRNA decreased AKT phosphorylation. Network analysis of the targeted genes above the 1.4 *z*-score cutoff revealed known upstream regulators of AKT, including EGFR (Harari and Yarden, 2000) and PKC (Li *et al.*, 1999), as decreasing pAKT S473 (Figure 4a). The only common interacting genes that when targeted decreased both pAKT S473 and T308 were AKT3 and GSK3 α (Figures 4a and b). We performed NetWalk analysis of the averaged data set and found that the only significant network is composed of receptors that are known to activate AKT and the GSK3 α -AKT1,3 subnetwork (Figure 4c). We further examined the relationship between AKT and GSK3 in the siRNA kinome screen. Analysis of the abundance of phosphorylated AKT and phosphorylated GSK3 showed a strong positive correlation coefficient of +0.7 between the paired proteins, which is expected, based on their known functional relationship. However, based on published literature, GSK3 α is proposed to be downstream of AKT (Manning and Cantley, 2007) and a role as an upstream regulator of pAKT was not expected. Nevertheless, we confirmed that knockdown of GSK3 α

using independent siRNA preparations does indeed block phosphorylation of AKT induced by EGF (Figure 4d). Experiments with GSK3 α or β knockout MEFs validated this connection between AKT and GSK3 α as EGF-induced AKT phosphorylation was markedly decreased in GSK3 α -knockout as compared with wild-type MEFs (Figure 4e). Previous reports show that GSK3 can regulate TSC2 activity (Inoki *et al.*, 2006); therefore we determined if TSC2 is involved in the GSK3 regulation of AKT phosphorylation. Silencing GSK3 in TSC2-null and wild-type MEFs decreased pAKT (Figure 4f), suggesting that the connection between GSK3 and AKT is independent of TSC2.

Discussion

The kinase and kinase-associated siRNA screen coupled to a high-throughput functional proteomics platform revealed differences in connectivity of the network of kinases that alter AKT phosphorylation at Thr 473 and Ser 308 (Figures 1b and c, and 4a and b). Identification of the previously known regulatory loops from mTOR and MAPK shows that unbiased systematic interrogation of the network is highly valuable in uncovering regulators of network function. Analysis of the two loops suggests regulation of AKT via pathways with differential dependence on p70S6K activity. The screen also identified an anti-correlation between phosphorylation of MAPK1,2 and AKT, suggesting that the activities of MAPK and AKT and their corresponding pathways are counterbalanced, maintaining homeostasis in the cell. Indeed, this counterbalance may contribute to the coordinated regulation of the AKT and MAPK pathways in cancer. For example, RAS mutations that activate both the MAPK pathway and PI3K/AKT pathway are usually seen in the absence of other mutations in the pathway, whereas mutations in dedicated pathway members, such as RAF and PIK3CA or PTEN, are commonly coordinated. This also suggests that targeting the PI3K, MAPK or mTOR pathways could be counterbalanced by activation of the other pathway and that coordinated inhibition of several pathways will be necessary for optimal therapeutic potential to be manifest. We identified a new functional relationship between AKT and GSK3 α and can now position GSK3 α both downstream and upstream of AKT, such that knockdown of GSK3 α decreases AKT phosphorylation induced by EGF. A recent study used a similar siRNA knockdown approach with an assessment of only three proteins by RPPA: pERK, pSTAT3 and actin, and identified a number of unexpected links between the EGFR and pERK (Komurov *et al.*, 2010a). Thus a systems approach combining knockdown of targets by siRNA with high-throughput quantitative analysis of functional proteomics can increase our understanding of the signaling networks and particularly cross-talk present in cells and may greatly aid in the development and implementation of targeted therapeutics.

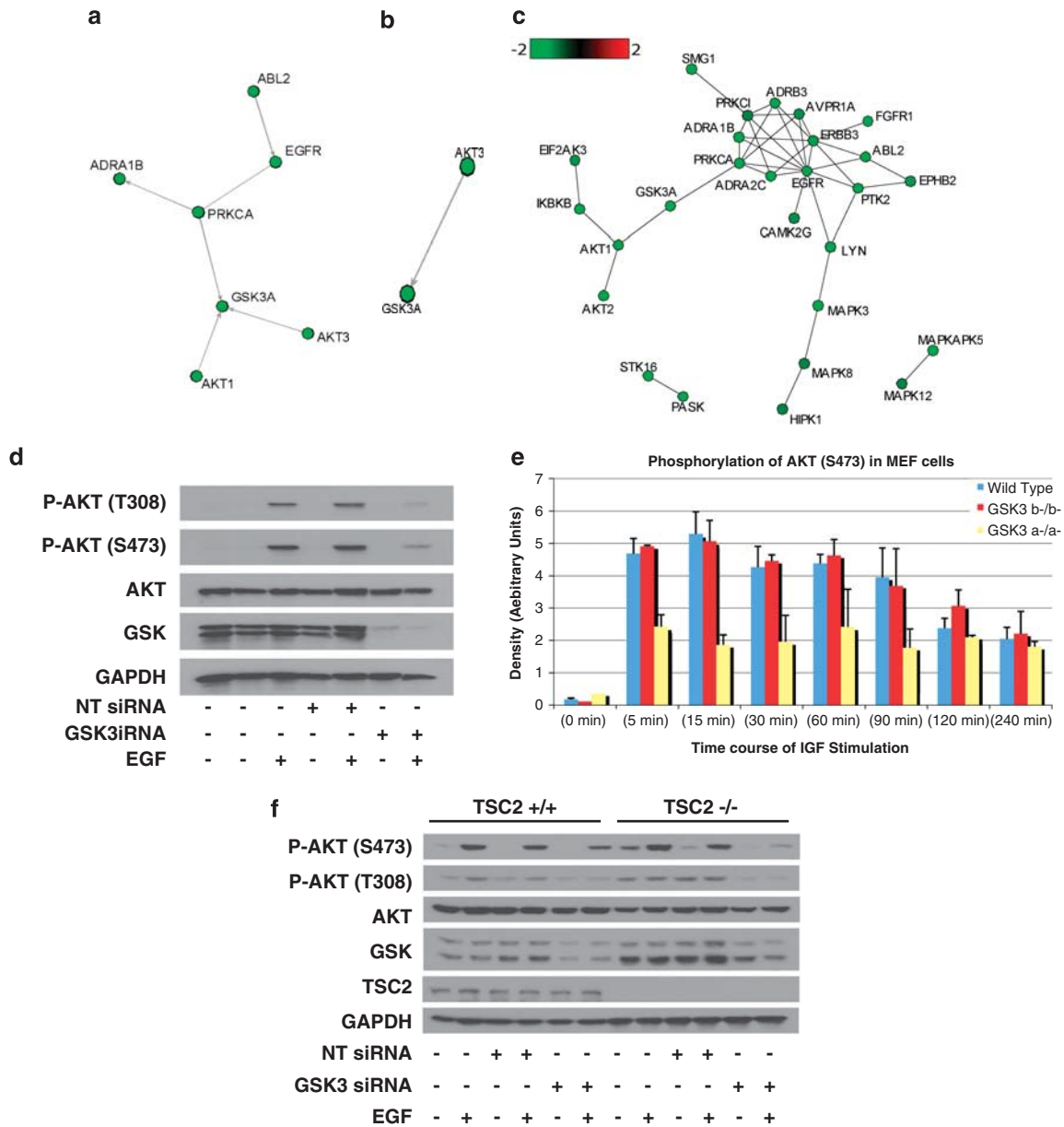


Figure 4 (a) Network of genes that when targeted by siRNA decreased phospho-Ser473 AKT below -1.7 z-score. (b) Only two known interacting genes were found of the genes that when targeted by siRNA decreased phospho-Thr308 AKT below -1.7 z-score. (c) The most low scoring network from the NetWalk analysis of the genes that when targeted by siRNA decreased Ser473 and Thr308 AKT phosphorylation. (d) GSK3 knockdown in MDA-MB-231 cells inhibits AKT phosphorylation. GSK3 was knocked down in MDA-MB-231 cells using SMARTpool siRNA. Cells were stimulated with EGF for 10 min and the lysates probed for phosphorylated AKT as indicated. (e) GSK3 α ^{-/-} MEFs show a blunted AKT response. MEFs from GSK3 α -deficient (GSK3 α -/ α -), GSK3 β -deficient (GSK3 β -/ β -) or wild-type animals were serum starved and stimulated with IGF for different lengths of time. Cell lysates were probed for phosphorylated AKT, showing the average and standard deviation of three independent experiments. (f) GSK3 α / β was silenced in wild-type and TSC2 knockout MEF cells. The cells were stimulated with EGF for 10 min and the lysates probed for phosphorylated AKT, total AKT, TSC2 and GSK3 as indicated.

Materials and methods

siRNA library screen by RPPAs

siRNA library targeting 541 kinases and kinase-related genes was designed by Dharmacon Research, Inc. (Lafayette, CO, USA), using their proprietary algorithm whereby each mRNA is targeted by a pool of siRNAs consisting of a combination of four siRNA duplexes directed at different regions of the gene.

This siRNA library has been previously characterized extensively by us (Morgan-Lappe *et al.*, 2006, 2007; Lin *et al.*, 2007; Sarthy *et al.*, 2007; Tahir *et al.*, 2007; Zheng *et al.*, 2008). The breast cancer cell line MDA-MB-468 (mutant PTEN, RB1, TP53 and SMAD4 and overexpressing EGFR) was seeded in 96-well plates at a density of 10 000 cells per well. Cells were transfected with 100 nm of the pool of siRNA consisting of 25 nm of each siRNA targeting each gene in each well by Mirus

TransIT TKO reagent (Mirus Bio LLC, Madison, WI, USA). Triplicate plates were performed with each plate containing the same set of controls including mock transfection, siRNA targeting polo-like kinase as a positive control, scrambled siRNA as a negative control, siTOX as a marker for siRNA delivery and staurosporin as a broad-kinase inhibitor. Forty-eight hours after siRNA transfection, cells were serum-starved overnight. Toxicity and cell death after siRNA transfection were measured using the Toxilight assay (Cambrex Corporation, East Rutherford, NJ, USA) according to the manufacturer's instructions, and siRNAs with marked toxicity were removed from the analysis. Cells were either unstimulated or stimulated with EGF (20 ng/ml) for 10 min before washing in PBS, then were lysed in 1% Triton X-100, 50 mM HEPES, pH 7.4, 150 mM NaCl, 1.5 mM MgCl₂, 1 mM EGTA, 100 mM NaF, 10 mM Na pyrophosphate, 1 mM Na₃VO₄ and 10% glycerol, containing freshly added protease and phosphatase inhibitors. Cellular proteins were denatured by 1% SDS (with β-mercaptoethanol) and diluted in six twofold serial dilutions in dilution buffer (lysis buffer containing 1% SDS). Serial diluted lysates were arrayed on nitrocellulose-coated FAST slides (Whatman, Inc., Piscataway, NJ, USA) by G3 Arrayer (Genomic Solutions, Huntingdon, UK). In total, 960 array spots were arranged on each slide, including 96 spots corresponding to positive and negative controls prepared from mixed cell lysates or dilution buffer, respectively. Each slide was probed with a validated primary antibody plus a biotin-conjugated secondary antibody. The signal was amplified using a DakoCytomation-catalyzed system (Dako, Carpinteria, CA, USA) and visualized by DAB colorimetric reaction. The slides were scanned, analyzed and quantified using a customized-software Microvigene (VigeneTech Inc., Carlisle, MA, USA) to generate spot intensity. Each dilution curve was fitted with the logistic model ('Supercurve Fitting' developed by the Department of Bioinformatics and Computational Biology in MD Anderson Cancer Center, <http://bioinformatics.mdanderson.org/OOMPA>). The program fits a single curve using all the samples (that are in the dilution series) on a slide with the signal intensity as the response variable and the dilution steps as the independent variable. The protein concentrations of each set of slides were then normalized by median polish, which was corrected across samples by the linear expression values using the median expression levels from all antibody experiments to calculate a loading correction factor for each sample.

Detection of AKT phosphorylation in MEF cell lines by RPPA
MEF cell lines differentially expressing wild-type GSK3α and β isoforms, GSK3β^{-/-} or GSK3α^{-/-} were kindly provided by Dr Jim Woodgett (University of Toronto). Cells were seeded in 12-well plates at 100 000 cells per well. Cells were serum starved overnight before stimulation with IGF at 75 ng/ml for 10, 30, 60, 120 and 240 min. Unstimulated cells were used as a control and designated as '0' minute. Triplicates were performed for each treatment. Cells were lysed and the lysates were denatured by 1% SDS as described above. Cellular proteins were serially diluted for five twofold dilutions and arrayed on nitrocellulose-coated Fast Slide by Aushon 2470 Arrayer (Aushon BioSystems, Inc, Billerica, MA, USA). The slide was probed by anti-pAKT (S473) and the data were analyzed as described above. The intensity of AKT phosphorylation was presented in a bar graph as the average plus standard deviation from the triplicates of each treatment.

Antibody validation for reverse-phase protein arrays

Antibodies with a single or dominant band on western blotting were further assessed by direct comparison with

RPPA using cell lines with differential protein expression or modulated with ligands or inhibitors of siRNA for phosphorylated or structural proteins, respectively. Only antibodies with a Pearson correlation coefficient between RPPA and western blotting of >0.7 were used in RPPA study. Further, these antibodies were assessed for specificity and quantification using phosphopeptides and non-phosphorylated peptides arrayed on nitrocellulose-coated slides (Supplementary Table 2).

Cell culture and stimulation

Human MDA-MB-231 breast cancer cells were maintained in RPMI supplemented with 10% FBS. Cells were serum starved for 16 h and then subjected to treatments using U0126 (MEK inhibitor) (10 μM) (Promega, Madison, WI, USA), EGF (20 ng/ml) (Cell Signaling Technology, Beverly, MA, USA) or both. MDA-MB-231 cells were transfected with 20 nM SMARTpool siRNA (Thermo Fisher Scientific Products, Dharmacon, Lafayette, CO, USA) for 72 h and stimulated with EGF (20 ng/ml) for 10 min. Cells were lysed and probed for phosphorylated AKT. For cells exposed to both reagents, the cells were pretreated with U0126 for 1 h followed by EGF stimulation for 10 min. Controls were incubated for the corresponding times with dimethyl sulfoxide (DMSO). For some experiments, cells were treated with siRNA for 72 h before treatment with knockdown TSC2 or MEK (Dharmacon Research Inc.).

SDS-PAGE and immunoblotting

Cells were lysed by incubation on ice for 15 min in a sample lysis buffer (50 mM Hepes, 150 mM NaCl, 1 mM EGTA, 10 mM sodium pyrophosphate, pH 7.4, 100 mM NaF, 1.5 mM MgCl₂, 10% glycerol and 1% Triton X-100 plus protease inhibitors: aprotinin, bestatin, leupeptin, E-64 and pepstatin A). Cell lysates were centrifuged at 15 000 g for 20 min at 4 °C. The supernatant was frozen and stored at -20 °C. Protein concentrations were determined using a protein-assay system (BCA, Bio-Rad, Hercules, CA, USA), with BSA as a standard. For immunoblotting, proteins (25 μg) were separated by SDS-PAGE and transferred to Hybond-C membrane (GE Healthcare, Piscataway, NJ, USA). Blots were blocked for 60 min and incubated with primary antibodies overnight, followed by goat antibody against mouse IgG-HRP (1:30 000; Cell Signaling Technology, Boston, MA, USA) or goat antibody against rabbit IgG-HRP (1:10 000; Cell Signaling Technology, Boston, MA, USA) for 1 h. Secondary antibodies were detected by enhanced chemiluminescence (ECL) reagent (GE Healthcare). All experiments were repeated a minimum of three independent times. The following antibodies were used for immunoblotting: antibody against phosphorylated p44 and p42 MAPKs, antibody against phosphorylated GSK3α/β (residues Ser²¹ and Ser⁹); antibody against phosphorylated AKT (residue Ser⁴⁷³); antibody against phosphorylated TSC2 (residue Thr¹⁴⁶²); antibody against phosphorylated mTOR (residue Ser²⁴⁴⁸); antibody against phosphorylated P70S6K (residue Thr³⁸⁹) (Cell Signaling Technology, Boston, MA, USA); and antibody against β-actin (Sigma-Aldrich, St Louis, MO, USA).

PathwayOracle network building

PathwayOracle (Ruths *et al.*, 2008a, b), was used to overlay the measured AKT phosphorylation on the network connectivity map derived from Science Signaling database of connections (<http://stke.sciencemag.org/cm/>) as well as from the network by Ma'ayan *et al.* (2005).

NetWalk analysis

We performed NetWalk analysis (Komurov *et al.*, 2010a,b) to identify networks of genes that when targeted by siRNA increased or decreased AKT phosphorylation in a coordinated manner. The algorithm uses data-biased random walks on graphs to identify interactions that are more significant than others as determined by both the data values as well connectivity. The algorithm has recently been published and is explained in detail in our recent paper (Komurov *et al.*, 2010a, b).

Conflict of interest

The authors declare no conflict of interest.

References

- Amit I, Citri A, Shay T, Lu Y, Katz M, Zhang F *et al.* (2007). A module of negative feedback regulators defines growth factor signaling. *Nat Genet* **39**: 503–512.
- Avruch J, Hara K, Lin Y, Liu M, Long X, Ortiz-Vega S *et al.* (2006). Insulin and amino-acid regulation of mTOR signaling and kinase activity through the Rheb GTPase. *Oncogene* **25**: 6361–6372.
- Ballif BA, Roux PP, Gerber SA, MacKeigan JP, Blenis J, Gygi SP. (2005). Quantitative phosphorylation profiling of the ERK/p90 ribosomal S6 kinase-signaling cassette and its targets, the tuberous sclerosis tumor suppressors. *Proc Natl Acad Sci USA* **102**: 667–672.
- Berns K, Horlings HM, Hennessy BT, Madiredjo M, Hijmans EM, Beelen K *et al.* (2007). A functional genetic approach identifies the PI3K pathway as a major determinant of trastuzumab resistance in breast cancer. *Cancer Cell* **12**: 395–402.
- Brugge J, Hung MC, Mills GB. (2007). A new mutational AKTivation in the PI3K pathway. *Cancer Cell* **12**: 104–107.
- Buck E, Eyzaguirre A, Rosenfeld-Franklin M, Thomson S, Mulvihill M, Barr S *et al.* (2008). Feedback mechanisms promote cooperativity for small molecule inhibitors of epidermal and insulin-like growth factor receptors. *Cancer Res* **68**: 8322–8332.
- Engelman JA, Luo J, Cantley LC. (2006). The evolution of phosphatidylinositol 3-kinases as regulators of growth and metabolism. *Nat Rev Genet* **7**: 606–619.
- Hanahan D, Weinberg RA. (2000). The hallmarks of cancer. *Cell* **100**: 57–70.
- Harari D, Yarden Y. (2000). Molecular mechanisms underlying ErbB2/HER2 action in breast cancer. *Oncogene* **19**: 6102–6114.
- Hennessy BT, Smith DL, Ram PT, Lu Y, Mills GB. (2005). Exploiting the PI3K/AKT pathway for cancer drug discovery. *Nat Rev Drug Discov* **4**: 988–1004.
- Hunter T. (2000). Signaling—2000 and beyond. *Cell* **100**: 113–127.
- Iadevaia S, Lu Y, Morales FC, Mills GB, Ram PT. (2010). Identification of optimal drug combinations targeting cellular networks: integrating phospho-proteomics and computational network analysis. *Cancer Res* **70**: 6704–6714.
- Inoki K, Ouyang H, Zhu T, Lindvall C, Wang Y, Zhang X *et al.* (2006). TSC2 integrates Wnt and energy signals via a coordinated phosphorylation by AMPK and GSK3 to regulate cell growth. *Cell* **126**: 955–968.
- Komurov K, Padron D, Cheng T, Roth M, Rosenblatt KP, White MA. (2010a). Comprehensive mapping of the human kinome to epidermal growth factor receptor signaling. *J Biol Chem* **285**: 21134–21142.
- Komurov K, White MA, Ram PT. (2010b). Use of data-biased random walks on graphs for the retrieval of context-specific networks from genomic data. *PLoS Comput Biol* **6**: e1000889.
- Kwiatkowski DJ, Manning BD. (2005). Tuberous sclerosis: a GAP at the crossroads of multiple signaling pathways. *Hum Mol Genet* **14**(Spec No. 2): R251–R258.

Acknowledgements

We thank Drs Kwiatkowski and J Woodgett for the knock out TSC2 and GSK3 cells, respectively. This study was funded in part by the Kleberg Center for Molecular Markers, the Komen Foundation, Stand Up to Cancer/American Association for Cancer Research Dream Team Translational Cancer Research Grant, Grant No. SU2C-AACR- DT0209, NIH CCSG P30CA16672, NIH Foundation DPA86424-444938 to BD and GBM, NIH CCTS support to DS, NIH T90DK070109 fellowship to J-TT and SI, Komen fellowship KG101547 to KK and PTR, DOD BC044268 and NIH R01CA125109 to PTR, NIH P01CA099031 and P50CA083639 to GBM, and U54 CA112970 to PTR and GBM. LN was supported by the Seed Funding Program Collaborative Advances in Biomedical Computing (CAMC), funded by the John and Ann Doerr Fund for Computational Biomedicine.

- Li W, Zhang J, Flechner L, Hyun T, Yam A, Franke TF *et al.* (1999). Protein kinase C- α overexpression stimulates Akt activity and suppresses apoptosis induced by interleukin 3 withdrawal. *Oncogene* **18**: 6564–6572.
- Lin X, Morgan-Lappe S, Huang X, Li L, Zakula DM, Vernetti LA *et al.* (2007). Seed analysis of off-target siRNAs reveals an essential role of Mcl-1 in resistance to the small-molecule Bcl-2/Bcl-XL inhibitor ABT-737. *Oncogene* **26**: 3972–3979.
- Ma'ayan A, Jenkins SL, Neves S, Hasseldine A, Grace E, Dubin-Thaler B *et al.* (2005). Formation of regulatory patterns during signal propagation in a mammalian cellular network. *Science* **309**: 1078–1083.
- Ma L, Chen Z, Erdjument-Bromage H, Tempst P, Pandolfi PP. (2005). Phosphorylation and functional inactivation of TSC2 by Erk implications for tuberous sclerosis and cancer pathogenesis. *Cell* **121**: 179–193.
- MacKeigan JP, Murphy LO, Blenis J. (2005). Sensitized RNAi screen of human kinases and phosphatases identifies new regulators of apoptosis and chemoresistance. *Nat Cell Biol* **7**: 591–600.
- Manning BD, Cantley LC. (2007). AKT/PKB signaling: navigating downstream. *Cell* **129**: 1261–1274.
- Manning BD, Logsdon MN, Lipovsky AI, Abbott D, Kwiatkowski DJ, Cantley LC. (2005). Feedback inhibition of Akt signaling limits the growth of tumors lacking Tsc2. *Genes Dev* **19**: 1773–1778.
- Morgan-Lappe S, Woods KW, Li Q, Anderson MG, Schurdak ME, Luo Y *et al.* (2006). RNAi-based screening of the human kinome identifies Akt-cooperating kinases: a new approach to designing efficacious multitargeted kinase inhibitors. *Oncogene* **25**: 1340–1348.
- Morgan-Lappe SE, Tucker LA, Huang X, Zhang Q, Sarthy AV, Zakula D *et al.* (2007). Identification of Ras-related nuclear protein, targeting protein for xenopus kinesin-like protein 2, and stearyl-CoA desaturase 1 as promising cancer targets from an RNAi-based screen. *Cancer Res* **67**: 4390–4398.
- Muller M, Obeyesekere M, Mills GB, Ram PT. (2008). Network topology determines dynamics of the mammalian MAPK1,2 signaling network: bifan motif regulation of C-Raf and B-Raf isoforms by FGFR and MC1R. *FASEB J* **22**: 1393–1403.
- Neve RM, Chin K, Fridlyand J, Yeh J, Baehner FL, Fevr T *et al.* (2006). A collection of breast cancer cell lines for the study of functionally distinct cancer subtypes. *Cancer Cell* **10**: 515–527.
- O'Reilly KE, Rojo F, She QB, Solit D, Mills GB, Smith D *et al.* (2006). mTOR inhibition induces upstream receptor tyrosine kinase signaling and activates Akt. *Cancer Res* **66**: 1500–1508.
- Roux PP, Ballif BA, Anjum R, Gygi SP, Blenis J. (2004). Tumor-promoting phorbol esters and activated Ras inactivate the tuberous sclerosis tumor suppressor complex via p90 ribosomal S6 kinase. *Proc Natl Acad Sci USA* **101**: 13489–13494.
- Ruths D, Muller M, Tseng JT, Nakhleh L, Ram PT. (2008a). The signaling petri net-based simulator: a non-parametric strategy for

- characterizing the dynamics of cell-specific signaling networks. *PLoS Comput Biol* **4**: e1000005.
- Ruths D, Nakhleh L, Ram PT. (2008b). Rapidly exploring structural and dynamic properties of signaling networks using PathwayOracle. *BMC Syst Biol* **2**: 76.
- Sarthy AV, Morgan-Lappe SE, Zakula D, Verneti L, Schurdak M, Packer JC *et al.* (2007). Survivin depletion preferentially reduces the survival of activated K-Ras-transformed cells. *Mol Cancer Ther* **6**: 269–276.
- Song JJ, Lee YJ. (2005). Dissociation of Akt1 from its negative regulator JIP1 is mediated through the ASK1-MEK-JNK signal transduction pathway during metabolic oxidative stress: a negative feedback loop. *J Cell Biol* **170**: 61–72.
- Tahir SK, Yang X, Anderson MG, Morgan-Lappe SE, Sarthy AV, Chen J *et al.* (2007). Influence of Bcl-2 family members on the cellular response of small-cell lung cancer cell lines to ABT-737. *Cancer Res* **67**: 1176–1183.
- Tibes R, Qiu Y, Lu Y, Hennessy B, Andreeff M, Mills GB *et al.* (2006). Reverse phase protein array: validation of a novel proteomic technology and utility for analysis of primary leukemia specimens and hematopoietic stem cells. *Mol Cancer Ther* **5**: 2512–2521.
- Wan X, Harkavy B, Shen N, Grohar P, Helman LJ. (2007). Rapamycin induces feedback activation of Akt signaling through an IGF-1R-dependent mechanism. *Oncogene* **26**: 1932–1940.
- Zheng M, Morgan-Lappe SE, Yang J, Bockbrader KM, Pamarthy D, Thomas D *et al.* (2008). Growth inhibition and radiosensitization of glioblastoma and lung cancer cells by small interfering RNA silencing of tumor necrosis factor receptor-associated factor 2. *Cancer Res* **68**: 7570–7578.

Supplementary Information accompanies the paper on the Oncogene website (<http://www.nature.com/onc>)